

**INTERACTION OF BALLOON CATHETER-STENT SYSTEMS  
WITH ATHEROSCLEROTIC LESIONS:  
A COMPUTATIONAL STUDY**

**Gerhard A. HOLZAPFEL<sup>1,2</sup> and Dimitrios E. KIOUSIS<sup>1</sup>**

<sup>1</sup>Institute of Biomechanics, Center of Biomedical Engineering  
Graz University of Technology, Kronesgasse 5-I, 8010 Graz, Austria

E-Mail: holzapfel@tugraz.at      URL: www.biomech.tugraz.at

<sup>2</sup>Department of Solid Mechanics, School of Engineering Sciences  
Royal Institute of Technology (KTH), Stockholm, Sweden

Appeared as a 'Book Chapter' in:

N. Chakfé and B. Durand (eds.), 'ESVB 2009 - New Technologies in Vascular Biomaterials.  
Connecting Biomaterials to Arterial Structures', Chapter 7,  
Europrot, Strasbourg, France (2009), 89-111.

## ABSTRACT

*A methodology is proposed that identifies optimal stent devices for specific clinical criteria. It enables to predict the effect of stent designs on the mechanical environment of stenotic arteries. In particular, we show representative experimental results of the transient expansion of a commercially available balloon-expandable stent system and a computational analysis of that system with a patient-specific atherosclerotic iliac artery.*

*Using a pneumatic-hydraulic experimental setup, the pressure-diameter diagram for a balloon-expandable stent is documented as well as typical measures such as the burst opening pressure, the maximum dog-boning and foreshortening, and the elastic recoil. The geometric arterial model is based on magnetic resonance images, while anisotropic material models are applied to describe the mechanical responses of the (four different) tissues at finite strains. In the simulations three different stent designs are studied. The performance of each stent is characterized by scalar quantities relating to stress changes in the artery, contact forces and changes in lumen area after stenting. The study concludes by suggesting two optimal stent designs for two different clinically relevant parameters.*

## INTRODUCTION

Balloon angioplasty with stenting is a well established and effective vascular reconstructive procedure aiming to reduce the severity of atherosclerotic stenosis, one of the most frequent form of cardiovascular diseases. Its popularity arises due to its less invasive nature (compared to surgical alternatives) and its better clinical outcome (compared to balloon angioplasty without stenting.<sup>11,34</sup>)

Despite the constantly increasing success rate of stenting through technological progresses in stent design and drug coatings on the stents' surface,<sup>4</sup> the procedure can still fail because of in-stent restenosis which occurs in 30-60% of patients with complex lesions.<sup>9</sup> Restenosis is a mechanobiological process characterized by stress-induced growth, such as neointimal hyperplasia. In more detail, the focal vascular trauma imposed by the struts of the stent, the stress and strain environments around the expanded stent, and the existence of a foreign material in the injured artery may trigger molecular mechanisms, leading to inflammation, granulation and extracellular matrix production.<sup>33,38,39</sup> These processes may lead to reclosure of the blood vessel, which results in the need for further interventions.

Balloon angioplasty with stenting is a procedure of mainly mechanical characteristics. It is, therefore, understandable that its outcome depends on, for example, the design parameters defining the mechanics of the stent such as the material and the geometry of stent cells and struts. This is supported by recent clinical studies,<sup>23,32</sup> which identified the stents' geometric characteristics as one of the major elements for reducing or increasing the risk of restenosis. Towards this direction, computational tools such as the finite element method have been used to investigate the biomechanical implications of vascular stenting and to provide optimal con-

figurations of medical devices.

This chapter reviews an experimental setup to study the inflation of balloon-expandable stents and to record related load and deformation including measures such as the burst opening pressure, maximum dog-boning and foreshortening, and elastic recoil. It briefly discusses the change of the inner balloon pressure over time during inflation and deflation of an EXPRESS VASCULAR LD™ balloon-stent system and the change of the central diameter of the stent over the pressure.<sup>26</sup> In addition, this chapter reviews a computational study that aims to investigate the interaction of vascular stents with a human atherosclerotic lesion; in particular 3D morphological data of a type V atherosclerotic lesion<sup>35</sup> of an iliac artery are considered.<sup>24</sup> The arterial wall is modeled as a non-homogeneous solid, consisting of four different tissue components. The applied constitutive models are able to capture the nonlinear, anisotropic behavior of arterial tissues. A vascular stent is parameterized and two modified geometric designs are generated. A cylindrically orthotropic model is used in order to describe the anisotropic behavior of balloon catheters under internal pressure load. The computational model also attempts to provide a deeper insight into the dominating effect of plaque fissuring and dissection during stenting.<sup>5,28,29</sup> This is performed by introducing two (small) initial cracks near the edges of the plaque.

The study results in the identification of changes in the mechanical environment of the artery during and after stenting, when the three different stent designs are used. Particular emphasis is placed on the generated stress fields of the four arterial tissues. The performance of the different stents is quantified by means of three scalar indicators.<sup>18</sup> These indicators characterize the lumen gain and the arterial injury imposed by the stents. Therefore, they may be helpful in finding the optimal stent design for the particular stenosis and for specific optimization criteria.

## **EXPERIMENTAL STUDY**

The goal is to investigate the deformation mechanisms (change in diameter and length) of balloon-expandable stent systems under operational internal pressure that range between 0 and 12 bar. Inflation tests are examined for the burst opening pressure, dog-boning, foreshortening and elastic recoil. The experimental setup and procedure of the balloon catheter-stent inflation is briefly described. The deformation mechanisms are presented and a comparison between the performance of six commercially available balloon-expandable stent systems during and after the inflation and deflation is provided.

### *Experimental setup and procedure*

The experimental setup accommodates two tasks: (i) the application of a pressure load inside the balloon causing a dilation of the balloon expandable stent, and (ii) the measurement of the load and the related deformation of the catheter-stent system. A schematic representation of the setup is depicted in Fig. 1. It is a simple, low cost pneumatic-hydraulic system, enhanced by two computer units and a camera.

The first step of the experimental process is concerned with the fixation of the catheter-stent system which is clamped at locations far away from its upper and lower boundaries. This allowed free expansion of the balloon in all three directions (radial, axial, circumferential). In addition the removal of the air from the inflation tube and the balloon catheter is carried out. Sterile water is used as inflation medium and therefore, all air must initially be evacuated from the system. This preparatory task is here performed as in clinical practice. In short, a stopcock along with a syringe are attached to the catheter's inflation port. While the stopcock is open, negative pressure is applied through the syringe. When total vacuum is achieved in the inflation

lumen and balloon, the stopcock is closed and the syringe is removed. The flow of the sterile water into the balloon then takes place and the inflation of the balloon-stent system is initiated.

In order to gradually increase the pressure of the water a compressed gas accumulator is used. One side of the accumulator is connected to a tube containing pressurized nitrogen, while the other chamber of the accumulator contains the hydraulic fluid (sterile water). The two media are separated by an elastic diaphragm. The progressive opening of the regulating vent connected to the gas tube leads to the gradational increase of the water's pressure, constantly measured by a pressure transducer located next to the catheter inflation port. The recording of the transducer is considered equal to the inner balloon pressure, by regarding the hydraulic losses negligible, and is subsequently labeled as  $p_b$ . The computer unit PC 2 records the input from the pressure transducer (the inflation load) at one second intervals, and simultaneously sends a signal to the computer unit PC 1. Simultaneously, PC 1 triggers a CCD camera equipped with a magnifying lens which takes a photograph of the catheter-stent system under dilation. Three examples of the acquired photographs are given in Fig. 2, where the deformed configurations of the balloon-stent system (EXPRESS VASCULAR LD<sup>TM</sup>) at different inner balloon pressures are shown. Image analysis software (Scion Imaging) is employed for a detailed analysis of these data. Information such as the stent's diameter (at different positions, for example, at distal and central segments) and the total length at a specific pressure load is extracted.

### *Experimental results*

The characteristic pressure-diameter ( $p$ - $D$ ) diagrams (i.e., the change of the stent's diameter with applied pressure load), can be determined by analyzing the obtained image data. The  $p$ - $D$  diagram is a direct and comprehensive source of information concerning the deformation

characteristics of the balloon catheter-stent system; see Fig. 3 for the EXPRESS VASCULAR LD<sup>TM</sup> balloon-stent system. In particular, Fig. 3(I) shows the gradual change of the inner balloon pressure  $p_b$  over time  $t$ , while Fig. 3(II) shows the change of the central diameter  $D_{st,c}$  over  $p_b$  (the  $D_{st,c}$ -measure is indicated in Fig. 2).

The diagrams of Fig. 3 indicate that the dilation of the EXPRESS VASCULAR LD<sup>TM</sup> balloon-stent system can be basically divided into four phases. Initially, as the pressure load starts to act on the inner side of the balloon catheter, the balloon fits closely to the stent. During this phase (Ⓐ → Ⓑ) the stent deforms elastically and its central diameter  $D_{st,c}$  changes only slightly. This is not the case for the distal segments of the stent, where larger deformation is noted at the edges of the stent for the same pressure level ( $0 \leq p_b \lesssim 3$  bar). This behavior, called dog-boning (or bone effect), is due to a higher compliance at the ends of the stent structure, and is clearly visible in Fig. 2. Dog-boning may be defined as<sup>31</sup>

$$DB = \frac{D_{st,d} - D_{st,c}}{D_{st,d}}, \quad (1)$$

where  $D_{st,d}$  is the diameter of the distal segment, as indicated in Fig. 2.

When the load reaches a specific limit, say  $p_b^*$  (for the EXPRESS VASCULAR LD<sup>TM</sup>  $p_b^*$  is 2.90 bar, see Fig. 3(II)), the stent starts to expand significantly (phase Ⓑ → Ⓒ), and the stent approaches its nominal diameter in a few seconds. The plateau of Fig. 3(II) shows this deformation mechanism. The main cause of this rapid expansion, referred to as burst opening, is the initiation of plastic deformation in some stent areas. The slight pressure drop during this phase is a consequence of the burst opening. As expected, when the diameter of the stent increases, then the volume increases causing a pressure drop. Subsequently, a new phase of deforma-

tion takes place ( $\textcircled{c} \rightarrow \textcircled{d}$ ), wherein the balloon-expandable stent system stiffens significantly in the circumferential direction. A high pressure increase is recorded against a low stent dilation rate. The main cause of this stiffening behavior is plastic deformation of the stent and, most important, the deformation characteristics of the balloon catheter (as discussed later in the manuscript). Finally, the load is gradually removed (phase  $\textcircled{d} \rightarrow \textcircled{e}$ ) and the pressure is reduced to  $p_b = 0$  bar. The final diameter of the stent is smaller than its diameter at maximum pressure load. This reduction in size is a result of the stent's elastoplastic deformation and is referred to as *recoil*. The central radial recoil  $\text{RE}_c^{\text{rad}}$  may be given by the relationship

$$\text{RE}_c^{\text{rad}} = \frac{D_{\text{st},c}^{p_b^{\text{max}}} - D_{\text{st},c}^{p_b^0}}{D_{\text{st},c}^{p_b^{\text{max}}}}, \quad (2)$$

with  $D_{\text{st},c}^{p_b^{\text{max}}}$  indicating the diameter of the stent's central segment at maximum pressure and  $D_{\text{st},c}^{p_b^0}$  is the same diameter after deflation of the balloon. In the case of the EXPRESS VASCULAR LD<sup>TM</sup> stent, the recoil is approximately 1.5%, and therefore, not readily apparent in Fig. 3(II).

As was stated in the introduction, two important characteristic mechanisms of stent expansion are dog-boning and foreshortening. Dog-boning is observed in all investigated stents. Based on an EXPRESS VASCULAR LD<sup>TM</sup> stent, Fig. 4(I) shows the typical change of the dog-boning DB, according to eq. (1), as a function of the inner balloon pressure  $p_b$ . The effect becomes clear at a pressure close to the burst opening pressure of the distal segments. When the balloon pressure reaches the value  $p_b^* \approx 3$  bar (central segment burst opening load) the stent approaches an approximately cylindrical shape and the dog-boning diminishes. At higher pressure loads and after deflation of the balloon catheter, the dog-boning decreases to zero.

The foreshortening mechanism describes the axial contraction of the stent under dilation.

Foreshortening may be defined as<sup>31</sup>

$$\text{FS} = \frac{L_{\text{st,defo}} - L_{\text{st,unde}}}{L_{\text{st,defo}}}, \quad (3)$$

where  $L_{\text{st,defo}}$  and  $L_{\text{st,unde}}$  denote the deformed and the undeformed lengths of the stent, respectively. For the case of the EXPRESS VASCULAR LD<sup>TM</sup> stent, the change of foreshortening FS over inner balloon pressure  $p_b$  is depicted in Fig. 4(II). Due to the cylindrical geometry of the stent and the dog-boning, inflation of the balloon-stent system leads to a decrease in stent length. The shortening reaches its maximum value as the dog-boning reaches its maximum as well (Figs 4(I)-(II)), i.e. at the burst opening pressure load of the stent's distal segments. In addition, as the load increases to the stent's operational pressure ( $\approx 11$  bar), the stent elongates from its compressed configuration. Finally, the removal of the pressure load leads to an axial contraction of the stent (2% for the EXPRESS VASCULAR LD<sup>TM</sup> stent).

In Table 1, the burst opening pressure  $p_b^*$ , the maximum dog-boning  $\text{DB}_{\text{max}}$ , the maximum foreshortening  $\text{FS}_{\text{max}}$  and the final central radial recoil RE (in percent) are given for six commercially available stents. The EXPRESS VASCULAR LD<sup>TM</sup> shows the largest dog-boning due to its larger circumferential stretch relative to the other stents, while the Racer stent shows the only positive value of foreshortening. In the Racer stent the maximum central radial recoil was measured after balloon removal.

## GEOMETRIC AND MATERIAL MODELING

This section provides the geometric and material modeling aspects of the vessel wall and the involved medical devices, i.e. the stent and the balloon catheter. The section starts with a

description of the 3D arterial model based on image data, and introduces the adopted continuum formulation, which is able to incorporate the nonlinearity and anisotropy inherent in human tissues. Next, account of a stent model, based on a currently used product, is given and finally a cylindrically orthotropic material model is used to describe the deformation of angioplasty balloons under internal pressure.

### *Arterial model*

In the present computational study, a detailed geometric and physical model of an atherosclerotic-prone human external iliac artery (65 yrs, female) is considered. The regarded lesion is of type V characterized by prominent new fibrous connective tissue and a lipid core.<sup>35</sup> The 3D geometry of the arterial wall architecture was traced by means of high-resolution magnetic resonance imaging (MRI) and reconstructed by non-uniform rational B-splines (NURBS), as can be seen in Fig. 5(I). A detailed description of the procedure and the associated histological analyses, required to identify the underlying tissue types, is provided in the references.<sup>1,17</sup> The identification of the 3D tissue structure is regarded as an important aspect of the documented attempt, and it is a necessary prerequisite of meaningful simulations of balloon angioplasty with stenting. According to the classification proposed by Holzapfel et al.,<sup>17</sup> seven different tissue types are identified in the atherosclerotic arterial wall: adventitia (A), non-diseased media (M-nos), non-diseased intima (I-nos), fibrous cap (I-fc), fibrous intima at the medial border (I-fm), lipid pool (I-lp), and fibrous media (M-f). For the purpose of this study, M-nos and M-f are combined to one tissue component referred to as ‘media’ (M), and I-nos, I-fc and I-fm are combined to another component referred to as ‘intima’ (I). The consideration of all seven arterial tissues would require detailed information about the anisotropy of each individual tissue, as discussed

later in this chapter. From the complete arterial wall a section with length  $l_a = 1.4$  mm (which is also the smallest cell length of the stent) is considered, which incorporates four tissue types (see Fig. 5).

Balloon angioplasty and stenting frequently lead to fissuring and dissection of the atherosclerotic plaque,<sup>5</sup> which is thought to be one of the main mechanisms of lumen gain obtained through this procedure. A reliable prediction of the stress field of the stented arterial wall requires the incorporation of these effects. However, the present work does not investigate the fissuring and dissection from a fracture mechanics point of view,<sup>10</sup> instead two initial tears (ITs) are introduced into the intima. The initial cracks are placed at the edges of the plaque (the plaque shoulder) because experimental studies indicate these locations as the most prominent ones to plaque rupture.<sup>28,29</sup> The arterial slice described above is depicted in Fig. 5(II).

For the determination of the passive, quasi-static mechanical properties of the individual tissue components, mechanical tests were performed on a computer-controlled, screw-driven, high-precision tensile machine. Rectangular stripe samples with axial and circumferential orientations were excised and stretched far beyond their physiological loading domain in order to capture the range of deformations induced by the stent. The lipid pool did not allow tensile testing due to its fluid-like consistency. A detailed description of the performed mechanical tests is documented in the study by Holzapfel et al.<sup>16</sup>

Arterial tissues are anisotropic, heterogeneous, highly deformable, (nearly) incompressible and show a pseudo-elastic behavior.<sup>15,20</sup> Following the work,<sup>14</sup> it is assumed that each tissue component is reinforced by two families of collagen fibers embedded in an isotropic ground matrix. This reinforcement renders the material properties anisotropic. The fibers' (mean)

preferred directions are represented by two unit vectors, say  $\mathbf{a}_{01}$  and  $\mathbf{a}_{02}$ . The isochoric part  $\bar{\Psi}$  of the strain energy stored in the non-collageneous and collageneous components is given by<sup>14</sup>

$$\bar{\Psi} = \bar{\Psi}(\bar{I}_1, \bar{I}_4, \bar{I}_6) = \mu(\bar{I}_1 - 3) + \frac{k_1}{2k_2} \sum_{i=4,6} \left\{ \exp \left[ k_2(\bar{I}_i - 1)^2 \right] - 1 \right\}, \quad (4)$$

where  $\bar{I}_1 = \text{tr} \bar{\mathbf{C}}$  is the first invariant of the modified Cauchy-Green tensor  $\bar{\mathbf{C}} = J^{-2/3} \mathbf{C}$ ,<sup>12</sup> and  $\bar{I}_4 = \bar{\mathbf{C}} : \mathbf{a}_{01} \otimes \mathbf{a}_{01}$  and  $\bar{I}_6 = \bar{\mathbf{C}} : \mathbf{a}_{02} \otimes \mathbf{a}_{02}$  are two invariants. The material parameters  $\mu$  and  $k_1$  have dimensions of stress, while  $k_2$  is a dimensionless parameter. The first part of (4)<sub>2</sub> models the contribution of the non-collageneous matrix, while the second part, characterizes the energy stored in the collagen fibers.

The strain energy described in (4) is used for each of the four tissue components, but with a different set  $(\mu, k_1, k_2)$  of material parameters, and different direction vectors ( $\mathbf{a}_{01}$  and  $\mathbf{a}_{02}$ ) associated with the structure. Up to now there are, unfortunately, no data available in the literature concerning the collagen structure of stenotic iliac arteries. In the present approach, the structural data  $\mathbf{a}_{01}$  and  $\mathbf{a}_{02}$  are treated phenomenologically and are estimated from the mechanical tests described previously. In addition, the components of the collagen fibers' direction vectors in the radial direction are neglected, allowing thus the description of  $\mathbf{a}_{01}$  and  $\mathbf{a}_{02}$  by an angle  $\alpha$ , defined between the fiber reinforcement and the circumferential direction of the individual layer. The least-square fitting of the constitutive model to the anisotropic data reported in the reference<sup>19</sup> leads to the determination of the three involved material parameters  $(\mu, k_1, k_2)$  and the structural parameter  $\alpha$ . The obtained values are summarized in Table 2. For more details of the material model (4) and suitable modifications see the book chapter.<sup>13</sup>

### *Stent models*

First we considered an EXPRESS VASCULAR LD<sup>TM</sup> stent with delivery system (guide wire and introducer sheath) obtained from Boston Scientific Sverige AB. The detailed shape and dimensions of the undeformed configuration of the stent, shown in Fig. 6(I), were studied using an Olympus reflected-light microscope with an attached digital camera.

The 3D computer model of the stent (Fig. 6(II)) is generated by means of a parametrization algorithm. Parametric design is a useful technique in engineering when products are tailored fit to specific needs or when optimization is used to generate the optimal product design. The algorithm makes use of a series of design parameters (see Fig. 6(II)), describing the stent's morphology and dimensions. In addition, the parametrization algorithm is able to provide the finite element mesh of the individual parameterized stent. In the simulations described below, three stent designs are taken into consideration. The first (control) stent, labeled as  $S_1$ , is the EXPRESS VASCULAR LD<sup>TM</sup> stent, with specific dimensions shown in Fig. 6(III)), while the two other designs derive from variations of the parameters defining the width of the struts ( $s_t$ ) and the wave length of the stent's cell ( $l_{st}$ ), see Table 3. The first variation of the control stent, labeled as  $S_2$ , has thinner struts (more compliant structure), while the second variation labeled as  $S_3$ , has approximately half of the struts of the control stent (stiffer structure). Since only a slice of the vessel wall is studied, only one cell of the stent is considered.

According to the acquired data, the EXPRESS VASCULAR LD<sup>TM</sup> stent is made of stainless steel (316L). The material's elastic regime is described by a neo-Hookean model, while its inelastic response is described by a von Mises-Hill plasticity model with linear hardening. The Young's modulus is  $E = 201$  GPa and the Poisson's ratio is  $\nu = 0.3$ . The yield stress  $\sigma_y$  is chosen equal to 300 MPa and the hardening modulus  $H_{iso}$  is equal to 2 GPa.

### *Balloon catheter models*

Although the initial form of balloon catheters is S- or Z-shaped, the undeformed configuration of the balloon is modeled as a circular cylinder. The outer diameter of the cylindrical balloon is  $D_{b,o} = 2.2$  mm, the thickness  $H_b = 0.2$  mm and the length  $l_b = 2.0$  mm.

The inflation of balloon catheters is characterized by complex kinematics.<sup>7</sup> Initially, the unfolding of the balloon takes place under low internal pressure. Further increase of the pressure, leads to a continuously increasing diameter, while the catheter retains axially its cylindrical shape. After a specific load, depending on the balloon's mechanical and geometric properties, the balloon exposes rapidly a nonlinear, stiffening behavior. In order to account for the described effects, a cylindrically orthotropic model, based on fiber-reinforced materials' theory, was used.<sup>25</sup> Briefly, two material axes with different mechanical properties are introduced, oriented in the axial and circumferential directions. Circumferentially, the balloon is very soft initially but particularly stiff after a predefined stretch limit, provided by the stent manufacturer. In the longitudinal direction the balloon is assumed to be already stiff at its reference direction, hence the axial stretch limit is about 1. The introduction of this artificial material allows the imitation of the typical characteristics of balloon catheters.<sup>25</sup> Note that this peculiar mechanical response could not be obtained by means of isotropic material models.

## **COMPUTATIONAL ANALYSIS**

This section summarizes the finite element model of balloon angioplasty with stenting, including the modeling of the contact interactions between the balloon, the stent and the arterial wall. The generation of the computational mesh is described as well as the boundary condi-

tions and the loading procedure. Finally, three indicators able to characterize the stent-artery interaction are discussed.

### *Finite element discretizations, contact modeling*

The 3D geometric models of the four arterial tissues are separately discretized by application of the commercial mesh generation toolkit CUBIT.<sup>6</sup> Approximately 3500 eight-node hexahedral elements are generated in total, and the mixed finite element formulation, implemented into the multipurpose finite element analysis program FEAP,<sup>37</sup> is applied. This approach provides an efficient and proper description of the incompressible deformation of arterial tissues. The meshes are generated with matching nodes on the tissue interfaces, and hence no special algorithmic treatment is required to link them. The same type of volume elements is chosen for the discretization of the balloon catheter, where 288 elements are generated. Finally, the structure of the stent implies the use of two-node, large displacement, large rotation 3D frame elements.<sup>21</sup> The choice of frame elements over hexahedral elements also leads to less computationally expensive simulations, an important aspect when complex contact problems are to be analyzed. The adopted contact algorithm is based on  $C^2$ -continuous uniform cubic B-spline surfaces documented in reference<sup>25</sup> and implemented in FEAP.

### *Boundary conditions*

Experience obtained through experimental investigations showed that, in contrast to healthy arteries, highly stenotic human vessels show very little or no axial *in situ* pre-stretch, approximately equal to 1 (a value of 1.03 is reported in reference<sup>16</sup>). Hence, no axial forces or displacements are applied to the artery. The top and bottom faces of the considered artery section are fixed in the axial direction (plane strain condition). The load-free configuration of the arterial

wall (shown in Fig. 5(II)) is also considered stress free, and hence residual strains (stresses) are neglected. Even though the algorithmic concept for the incorporation of residual stresses exists,<sup>36</sup> the lack of experimental data in atherosclerotic lesions makes their consideration not possible in this work. Next, a small value of stiffness is given to each node of the artery. This restricts the rigid motion of the artery. To obtain an almost concentric expansion of the balloon catheter, its nodes located on two orthogonal axial planes are fixed in the circumferential direction. As far as the stent is concerned, the axial displacements are fixed for all the nodes on its midplane, thus, restricting its rigid motion.

#### *Loading procedure*

The reference diameter of the chosen catheter and stent is bigger than the diameter of the lumen of the stenotic vessel under investigation. Hence, the undeformed balloon and stent are placed in the lumen with penetration. Next, the penalty parameter which enforces the contact constraint is gradually increased in a few load steps. Thus, the penetration is reduced and the contact between the medical devices and the inner arterial wall is established in a computationally stable way. The expansion of the balloon catheter follows. This is performed by follower pressure loads which are applied on the inner surface of the balloon. An increase of the inner balloon pressure leads to the expansion of the three bodies. When the outer diameter of the balloon reaches a desired value, the balloon contact penalty parameter is gradually decreased, simulating the balloon catheter's deflation, and only the plastically deformed stent remains in contact with the inner surface of the vessel.

#### *Indicators for the outcome of angioplasty*

Local stress distributions within the specimen during balloon angioplasty and stenting are

undoubtedly an important measure to illustrate the changes in the mechanical environment of the vessel wall caused by a particular stent. Nevertheless, if criteria are based on a set of scalar quantities and linked to mechanical measures such as contact forces and stresses, then they could provide a faster and more comprehensive and reliable judgment of the stent-stenosis interaction. The idea to introduce scalar indicators, characterizing the mechanical field of the arterial wall and the lumen change after stenting, was initially proposed in the reference,<sup>18</sup> while also applied in.<sup>3,25</sup>

The first indicator characterizes the contact force applied on the intimal surface from the stent's struts. This is an important measure, since elevated contact pressure in the vicinity of the stent struts may lead to injury of the endothelial and medial smooth muscle cells, which may increase the neointimal hyperplasia formation.<sup>27</sup> The indicator of the normalized contact forces at the intimal surface caused by the stent struts is denoted by  $D_1$ , and expressed as

$$D_1 = \sum_{i=1}^{n_s} \frac{F_{i,\text{post}}}{l_c}, \quad (5)$$

where  $n_s$  is the total number of nodes of the stent cell and  $F_{i,\text{post}}$  is the norm of the contact force at each stent node after stenting, given by

$$F_{i,\text{post}} = \left( \sum_{j=1}^3 f_j^2 \right)^{1/2}, \quad (6)$$

where  $f_j$  are the reaction force components at the node  $i$ , and  $l_c$  is the total length of the considered stent cell. The indicator  $D_1$  can also be used as a measure for prolapse, hence as a measure for the deflection of tissue between the struts. Prolapse, depends strongly on the artery's (ma-

terial) composition, the contact forces and the spacing between the stent struts, thus it can be linked to  $D_1$ . In addition, prolapse provides an important insight on the effectiveness of stenting since clinical studies relate it with the appearance of restenosis.<sup>22</sup>

As aforementioned, a critical factor that drives restenosis is the long-term change of stresses within the arterial wall after the performance of the interventional treatment. High stresses induced by the stent may be responsible for the triggering of growth mechanisms and finally may lead to restenosis.<sup>39</sup> Therefore, a second indicator  $D_2$  is used, able to quantify stress changes in the arterial wall. This indicator is defined as<sup>18</sup>

$$D_2 = \frac{\sum_{i=1}^{n_v} \Delta\sigma_i \Omega_i}{\sum_{i=1}^{n_v} \sigma_{i,\text{MAP}} \Omega_i}, \quad \Delta\sigma_i = \sigma_{i,\text{post}} - \sigma_{i,\text{MAP}}. \quad (7)$$

In the above equation,  $n_v$  denotes the number of the arterial volume elements and  $\Omega_i$  the volume of the element  $i$ , which is used as a weighting factor. Next,  $\sigma_{i,\text{post}}$  and  $\sigma_{i,\text{MAP}}$  are the maximum (principal) stress in the element  $i$  after stenting and under mean arterial pressure, respectively.

The last indicator, denoted by  $LG$  (**Lumen Gain**), corresponds to the lumen change due to stenting. The lumen gain  $LG$  is defined as<sup>18</sup>

$$LG = \frac{A_{\text{post}}}{A_{\text{MAP}}} - 1, \quad (8)$$

where  $A_{\text{MAP}}$  is the smallest inner cross-section of the artery before angioplasty and stenting, and  $A_{\text{post}}$  is the cross-section at the same location as  $A_{\text{MAP}}$  after angioplasty and stenting.

## RESULTS

In the following section, the most illustrious results of the performed computational simulations are provided. In particular, the stenting induced stress fields of the arterial tissues are studied and the performance of the considered stent designs is analyzed using scalar indicators.

### *Predicted stress fields*

The first of the performed simulations concerns the atherosclerotic lesion under internal pressure load. The chosen load is the mean arterial pressure taken to be  $p_{\text{MAP}} = 13.3 \text{ kPa}$ . Note that in this case no initial tears are incorporated since tissue dissection and fissuring are considered to take place at loadings which occur during balloon angioplasty. The stress field in this case is illustrated in Fig. 7(I). The maximum (principal) stresses are given in kPa and are shown for the intima, media and adventitia. As can be seen in Fig. 7(I), the innermost layer of the lesion is the main load carrier of the structure. The deformed state, as shown in Fig. 7(I), is regarded as the pre-stenting reference state, indicated by  $(\bullet)_{\text{MAP}}$ .

Next, the (small) initial cracks at the intima are considered and the deformed configuration and stress distribution in the arterial tissues under the same loading conditions are studied (Fig. 7(II)). As previously mentioned, the role of the tears is to incorporate fissuring and dissection of the arterial tissues, which occur during angioplasty interventions.<sup>5,28,29</sup> The above simulation aims to model the procedure of balloon angioplasty without stenting. The evolution of the crack tips due to the internal pressure is visible in Fig. 7(II).

The following step is concerned with the computational modeling of stenting with reference to the undeformed configuration of the stenotic lesion including the two initial tears. The three different stent designs, as introduced within the section ‘Stent models’, are used for this purpose.

Figures 7(III) and 7(IV) show the deformed shapes and the resulting stress fields at full balloon inflation and after deflation of the balloon catheter, respectively. Thereby the model of the ‘original’ (control) EXPRESS VASCULAR LD™ stent is used. In all cases the balloon is inflated until its outer diameter reaches the value  $d_{b,o} = 4.5$  mm, which corresponds to an approximate balloon internal pressure of  $p_b = 8$  bar. Then, the balloon is removed and only the stent remains in contact with the arterial wall. The slightly smaller lumen area, as shown in Fig. 7(IV), with respect to Fig. 7(III), reveals the recoil of the elastoplastic stent. As can be seen in the Figs 7(II-IV), the tear of the intima and its dissection from the media, lead to a different stress field (when compared to the condition depicted in Fig. 7(I)). In the case of balloon angioplasty without and with stenting, the intact intima continues to carry the main part of the load, but the stresses in the adventitia and media increase during and after stenting (especially behind and at the tips of the dissections). In particular, a value of approximately 500 kPa is obtained at both tips at full balloon inflation (Fig. 7(III)). According to Holzapfel et al.,<sup>17</sup> human atherosclerotic plaques of iliac arteries rupture at a stress level similar to that computed here, which additionally justifies the incorporation of the (small) initial cracks. It is interesting to observe that in the diseased part of the intima a stress-shield in form of an arc is present. The acquired results also point out that the lipid pool is under a low compressive hydrostatic pressure. The obtained deformed shapes and stress fields, as illustrated in Fig. 7(IV), qualitatively and quantitatively agree with the outcome of a recent study,<sup>10</sup> where plaque fissuring and dissection during angioplasty were modeled by means of a fracture propagation algorithm based on cohesive zones. However, therein, no stent is used and the analysis does not address contact interactions. Note that for all considered cases the highest stresses were obtained at the introduced crack tip.

*Comparison of different stent designs*

At the end of the performed simulations of balloon angioplasty without and with stenting using the three stent designs, the aforementioned indicators  $D_1$ ,  $D_2$ ,  $LG$  are computed for each case. The obtained values are then normalized (from 0 to 1) according to

$$\overline{\text{ind}} = \frac{\text{ind} - \text{ind}_{\min}}{\text{ind}_{\max} - \text{ind}_{\min}}, \quad (9)$$

where ‘ind’ stands for the indicator  $D_1$ ,  $D_2$ ,  $LG$ . The quantities  $\text{ind}_{\max}$  and  $\text{ind}_{\min}$  refer to the maximum and minimum values of the related indicator with respect to the four cases, i.e. ‘balloon angioplasty (no stent)’, ‘control stent  $S_1$ ’, ‘stent with thinner struts  $S_2$ ’ and ‘stent with fewer struts  $S_3$ ’, with parameters according to Table 3. From (9), it is obvious that  $\overline{\text{ind}} = 0$  corresponds to the minimum value of the indicator ind and  $\overline{\text{ind}} = 1$  to the maximum value. The normalized indicators  $\overline{D_1}$ ,  $\overline{D_2}$ ,  $\overline{LG}$  for each simulation are plotted in Fig. 8.

As expected, the lowest lumen gain is obtained for the case of balloon angioplasty, where no scaffold is present to keep the elastic artery open ( $LG = 18\%$  due to the tears which weaken the structure). Obviously, for this case  $D_1 = 0$  since no stent is present. The maximum values for  $LG$  are acquired when the control stent  $S_1$  ( $LG = 48\%$ ) and the stent with the fewer struts  $S_3$  ( $LG = 47\%$ ) are used. These two stent designs also lead to the highest values for the indicator  $D_2$ , which characterizes (arterial) stress changes. Generally, Fig. 8 reveals a strong correlation between the indicators  $LG$  and  $D_2$ . In other words, the induced stresses in the arterial tissues highly depend on the final dilated state of the artery. Among the three stents, the thinner and more compliant stent  $S_2$  results to the lowest values for all three indicators ( $LG = 42\%$ ). A comparison between the stents  $S_1$  and  $S_2$  indicates that by reducing the thickness of the struts

by 40%, the achieved lumen gain ( $LG$ ), the contact forces ( $D_1$ ) and the (arterial) stress changes ( $D_2$ ) reduce by approximately 25%. Remarkably, as can be seen in Fig. 8, stent  $S_3$  shows the highest  $\overline{D_1}$  value, hence it generates the highest contact forces on the intimal surface, while at the same time, exhibits comparable values for the indicators  $\overline{D_2}$  and  $\overline{LG}$  (1% difference) to the control stent  $S_1$ , as previously mentioned. This arises from the geometric characteristics of stent  $S_3$ , since a stent with fewer struts on its periphery is structurally stiffer than a stent with more struts and the same thickness. In the case of  $S_3$  a bigger prolapse value is also expected due to the larger distance between the struts.

It is clear that the above indicators stand for competing interests. An optimal treatment or stent design should, from a clinical point of view, lead to sufficiently enlarged lumen area (large  $LG$  values). At the same time, it should not induce unnecessary arterial trauma, or in other words, should minimize the changes in stresses of the arterial wall and should not apply high contact forces on the intimal surface (small  $D_1$  and  $D_2$  values). The importance of each indicator for an optimization procedure depends on the specific patient and the related patient history.

The results of the simulations performed in this work suggest that the control stent  $S_1$  leads to the most promising results in terms of lumen gain. The same  $LG$  can also be accomplished by the use of stent  $S_3$ . However,  $S_3$  results in more significant changes in the mechanical environment of the arterial wall expressed through  $D_1$ . Consequently,  $S_3$  produces more local damage of the intimal surface due to contact forces, for the same outcome. In the case where a stent design that minimizes arterial damage is more preferable over a stent that maximizes lumen gain, the thinner and more compliant stent  $S_2$  is the most appropriate device among

the other two. Stent  $S_2$  leads to lower values of the indicators  $D_1$  and  $D_2$ . Accepting that these scalar measures are linked to arterial tissue damage one may assume that stent  $S_2$  is, consequently, less prone to restenosis. This result is comparable with the outcome of clinical studies,<sup>23,32</sup> which identified that thinner struts elicit less angiographic restenosis than thicker struts.

## DISCUSSION AND CONCLUSION

A comprehensive computational model of the arterial wall, the medical devices and their contact interaction is of pressing need and of utmost importance for a deeper understanding of the vessel response under supra-physiological loading as occurring during and after stent placement. The availability of a comprehensive model is also important for the optimization of stent structures, and, therefore, of the interventional procedure which often fails due to biological reactions such as restenosis. In the present work the mechanical response of vascular balloon catheter-stent systems were experimentally analyzed during inflation. In addition, a methodology was proposed to identify ‘optimal’ stent devices. In particular, a computational framework able to identify the changes in the mechanical environment of atherosclerotic human lesions that occur due to the interaction with vascular stents was presented.

A pneumatic-hydraulic experimental setup was presented (Fig. 1) able to apply pressure inside of balloon catheters and to simultaneously record loads and deformed states of balloon-expandable stents during inflation. Postprocessing of experimentally obtained data and images (Fig. 2) makes it possible to extract characteristic pressure-diameter diagrams for individual stents, here shown for the EXPRESS VASCULAR LD<sup>TM</sup> balloon-stent system (Fig. 3). The

generated images and diagrams reveal that during inflation of the balloon-stent systems, the overall deformation path can be sub-divided into three characteristic phases, and phenomena such as dog-boning and foreshortening take place (Fig. 4). Table 1 summarizes additional information including the burst opening pressure, the maximum dog-boning and foreshortening values, and the elastic recoil. The experimental approach demonstrated a suitable basis for the better analysis of vascular balloon catheter-stent systems and for the development of new stent designs. The study identified stents with maximum values of dog-boning and foreshortening.

We analyzed a stenotic iliac artery in more detail and modeled it as a solid continuum composed of four types of tissues. The mechanical response of each tissue was described by a neo-Hookean material relating to the non-collagenous matrix, in addition to an anisotropic material, which relates to the response of the collagen fibers.<sup>14</sup> The different sets of material and structural parameters for each tissue were identified by means of *in vitro* uniaxial tensile tests<sup>19</sup> (see Table 2). Residual stresses were not incorporated into the model due to the lack of experimental data on atherosclerotic human iliac arteries. In order to account for the important inelastic effects of the artery at finite deformations such as plaque fissuring and dissipation, two initial tears were introduced into its load-free configuration at locations prone to crack initiation. In addition, the nonlinear and anisotropic mechanical response of the balloon catheter was described by a cylindrically orthotropic model.<sup>25</sup> An EXPRESS VASCULAR LD<sup>TM</sup> iliac stent was used for the generation of a computer stent model with a number of (flexible) geometric parameters. Two more stent models were generated, one with thinner struts and one with fewer struts (for related parameters see Table 3).

The interaction between the medical devices (balloon and stent) and the inner arterial wall

was solved as a 3D contact problem.<sup>25</sup> In order to keep the computational costs low only a 3D section of the arterial wall, one stent cell and the smallest cell length ( $l_a = 1.4$  mm) were considered. One simulation of balloon angioplasty without stent and three with a stent and the aforementioned different designs were performed. All computations showed that the incorporation of the tears at the intima led to a different (principal) stress environment in the stenosis. In particular, in that case, the mechanical load was carried by the intima, the non-diseased media and the adventitia. However, the highest stresses were reported at the vicinity of the tears, hence the induced trauma due to stenting remained localized at the dissection site rather than spreading over the lesion, which is in accordance with the study.<sup>10</sup>

Finally, scalar indicators were defined that allow an *objective* judgment on the performance of the used stents and their interactions with the specific atherosclerotic lesion. These indicators ( $D_1$ ,  $D_2$ ,  $LG$ ) are measures of the contact forces applied from the stent to the intimal surface, of the changes of the mechanical stresses in the individual tissues and of the achieved lumen gain. The results revealed a strong correlation between the lumen gain and the induced stress level. Among the different stent configurations,  $S_1$  and  $S_3$  showed comparable values of the indicators  $D_2$  and  $LG$ . Nevertheless, the stent  $S_3$  led to higher values of the contact forces ( $D_1$ ), being thus possibly a less favorable option for clinicians than the control stent  $S_1$ . The described method indicated that a choice for the most appropriate stent strongly depends on the optimization criterion. In the case that less vascular trauma was regarded as more important than higher lumen area, the performed simulations suggested stent  $S_2$  with the thinner struts as the optimal stent for the lesion under investigation.

There are some limitations of the study that should be addressed in the near future. The

balloon-stent systems were not experimentally tested in the application environment, i.e. inside an atherosclerotic arterial wall. The design of such an experiment could provide information on the damage induced by the stent struts on the endothelial layer. For a methodology to study the morphologic changes in lesions during *in vitro* angioplasty with balloon expansion see the study by, for example, Auer et al.<sup>2</sup> Crimping of the stent to the balloon catheter was not simulated, and hence the residual stresses and strains resulting from this procedure were not considered. It is noted, however, that the results of the study by De Beule et al.<sup>8</sup> show that the crimping procedure has a minor influence on the overall expansion of the stent. The undeformed configuration of the balloon catheter is considered to be uniform and cylindrical, and its folded shape is not modeled. However, the adopted nonlinear model manages to successfully simulate the unfolding phase of the balloon in a phenomenological way. In addition, the presented computational model did not incorporate microstructural effects of the stent. The average grain size of stainless steel is almost of the same order of magnitude as the stent's strut thickness (approximately  $150\ \mu\text{m}$ ). Therefore, a continuum mechanical model may be questionable. Note that the paper by McGarry et al.<sup>30</sup> analyzes micro-scale mechanical phenomena of the stent material behavior using physically based crystal plasticity theory rather than phenomenological plasticity theory. Refinements on the geometric and constitutive models have also to be considered in future studies. In particular, a larger-scale model should be studied, considering a representative unit length ( $a + b + c$ ) of the stent (see Fig. 6) or the stent as a whole, and the complete 3D morphology of the artery. A computational analysis on such a basis would lead to local stress concentrations in the non-diseased intima at the stent edges<sup>19</sup> depending on the lesion-morphology and the utilized stent type.

Apart from the mentioned limitations, the proposed experimental methodology and the physical and computational models have the ability to provide clear markers for the patient-specific choice of the optimal stent configuration and should be considered as a further step towards optimization of the stenting technique.

## References

- [1] M. Auer, R. Stollberger, P. Regitnig, F. Ebner, and G. A. Holzapfel. 3-D reconstruction of tissue components for atherosclerotic human arteries based on high-resolution MRI. *IEEE T. Med. Imaging*, 25:345–357, 2006.
- [2] M. Auer, R. Stollberger, P. Regitnig, F. Ebner, and G. A. Holzapfel. A methodology to study the morphologic changes in lesions during *in vitro* angioplasty using MRI and image processing. *Med. Image Anal.*, 12:163–173, 2008.
- [3] J. Bedoya, C. A. Meyer, L. H. Timmins, M. R. Moreno, and J. E. Moore Jr. Effects of stent design parameters on normal artery wall mechanics. *J. Biomech. Eng.*, 128:757–765, 2006.
- [4] H. M. Burton and W. L. Hunter. Drug-eluting stents: A multidisciplinary success story. *Adv. Drug Deliv. Rev.*, 58:350–357, 2006.
- [5] W. R. Castaneda-Zuniga, A. Formanek, M. Tadavarthy, Z. Vlodayer, J. E. Edwards, C. Zollikofer, and K. Amplatz. The mechanism of balloon angioplasty. *Radiology*, 135:565–571, 1980.

- [6] CUBIT Team. *CUBIT 10.0 User's Manual*. Sandia National Laboratories, Albuquerque, New Mexico, USA, 2005.
- [7] M. De Beule, P. Mortier, S. G. Carlier, B. Verhegghe, R. Van Impe, and P. Verdonck. Realistic finite element-based stent design: the impact of balloon folding. *J. Biomech.*, 41:383–389, 2008.
- [8] M. De Beule, P. Mortier, R. Van Impe, B. Verhegghe, P. Segers, and P. Verdonck. Plasticity in the mechanical behaviour of cardiovascular stents during stent preparation (crimping) and placement (expansion). *Key Eng. Mater.*, 340–341:847–852, 2007.
- [9] R. Fattori and T. Piva. Drug-eluting stents in vascular intervention. *Lancet*, 361:247–249, 2003.
- [10] T. C. Gasser and G. A. Holzapfel. Modeling plaque fissuring and dissection during balloon angioplasty intervention. *Ann. Biomed. Eng.*, 35:711–723, 2007.
- [11] M. Hoher, J. Wohrle, O. C. Grebe, M. Kochs, H. H. Osterhues, V. Hombach, and A. B. Buchwald. A randomized trial of elective stenting after balloon recanalization of chronic total occlusions. *J. Am. Coll. Cardiol.*, 34:722–729, 1999.
- [12] G. A. Holzapfel. *Nonlinear Solid Mechanics. A Continuum Approach for Engineering*. John Wiley & Sons, Chichester, 2000.
- [13] G. A. Holzapfel. Arterial tissue in health and disease: Experimental data, collagen-based modeling and simulation, including aortic dissection. In G. A. Holzapfel and R. W. Ogden, editors, *Biomechanical Modelling at the Molecular, Cellular and Tissue Levels*, pages 259–343, Wien, New York, 2009. Springer-Verlag. CISM Courses and Lectures no. 508.

- [14] G. A. Holzapfel, T. C. Gasser, and R. W. Ogden. A new constitutive framework for arterial wall mechanics and a comparative study of material models. *J. Elasticity*, 61:1–48, 2000.
- [15] G. A. Holzapfel and R. W. Ogden, editors. *Biomechanical Modelling at the Molecular, Cellular and Tissue Levels*. Springer-Verlag, Wien – New York, 2009.
- [16] G. A. Holzapfel, C. A. J. Schulze-Bauer, and M. Stadler. Mechanics of angioplasty: Wall, balloon and stent. In J. Casey and G. Bao, editors, *Mechanics in Biology*, New York, 2000. The American Society of Mechanical Engineers (ASME). AMD-Vol. 242/BED-Vol. 46, pp. 141–156.
- [17] G. A. Holzapfel, G. Sommer, and P. Regitnig. Anisotropic mechanical properties of tissue components in human atherosclerotic plaques. *J. Biomech. Eng.*, 126:657–665, 2004.
- [18] G. A. Holzapfel, M. Stadler, and T. C. Gasser. Changes in the mechanical environment of stenotic arteries during interaction with stents: Computational assessment of parametric stent design. *J. Biomech. Eng.*, 127:166–180, 2005.
- [19] G. A. Holzapfel, M. Stadler, and C. A. J. Schulze-Bauer. A layer-specific three-dimensional model for the simulation of balloon angioplasty using magnetic resonance imaging and mechanical testing. *Ann. Biomed. Eng.*, 30:753–767, 2002.
- [20] J. D. Humphrey. *Cardiovascular Solid Mechanics. Cells, Tissues, and Organs*. Springer-Verlag, New York, 2002.
- [21] A. Ibrahimbegović and M. Al Mikdad. Finite rotations in dynamics of beams and implicit time-stepping schemes. *Int. J. Numer. Meth. Engng*, 66:781–814, 1998.

- [22] I.-K. Jang, G. Tearney, and B. Bouma. Visualization of tissue prolapse between coronary stent struts by optical coherence tomography. Comparison with intravascular ultrasound. *Circulation*, 104:2754, 2001.
- [23] A. Kastrati, J. Mehilli, J. Dirschinger, F. Dotzer, H. Schühlen, F.-J. Neumann, M. Fleckenstein, C. Pfafferott, M. Seyfarth, and A. Schömig. Intracoronary stenting and angiographic results: strut thickness effect on restenosis outcome (ISAR-STEREO) trial. *Circulation*, 103:2816–2821, 2001.
- [24] D. E. Kiousis, T. C. Gasser, and G. A. Holzapfel. A numerical model to study the interaction of vascular stents with human atherosclerotic lesions. *Ann. Biomed. Eng.*, 35:1857–1869, 2007.
- [25] D. E. Kiousis, T. C. Gasser, and G. A. Holzapfel. Smooth contact strategies with emphasis on the modeling of balloon angioplasty with stenting. *Int. J. Numer. Meth. Engng*, 75:826–855, 2008.
- [26] D. E. Kiousis, A. Wulff, and G. A. Holzapfel. Experimental studies and numerical analysis of the inflation and interaction of vascular balloon catheter-stent systems. *Ann. Biomed. Eng.*, 37:315–330, 2009.
- [27] A. König, T. M. Schiele, J. Rieber, K. Theisen, H. Mudra, and V. Klaus. Influence of stent design and deployment technique on neointima formation and vascular remodeling. *Z. Kardiol.*, 91:98–102, 2002.
- [28] R. T. Lee, H. M. Loree, G. C. Cheng, E. H. Lieberman, N. Jaramillo, and F. J. Schoen. Computational structural analysis based on intravascular ultrasound imaging before *in*

*in vitro* angioplasty: Prediction of plaque fracture locations. *J. Am. Coll. Cardiol.*, 21:777–782, 1993.

[29] R. T. Lyon, C. K. Zarins, C. T. Lu, C. F. Yang, and S. Glagov. Vessel, plaque and lumen morphology after transluminal balloon angioplasty. Quantitative study in distended human arteries. *Arteriosclerosis*, 7:306–314, 1987.

[30] J. P. McGarry, B. P. O’Donnell, P. E. McHugh, and J. G. McGarry. Analysis of the mechanical performance of a cardiovascular stent design based on micromechanical modelling. *Comp. Mater. Sci.*, 31:421–438, 2004.

[31] F. Migliavacca, L. Petrini, M. Colombo, F. Auricchio, and R. Pietrabissa. Mechanical behavior of coronary stents investigated through the finite element method. *J. Biomech.*, 35:803–811, 2002.

[32] J. Pache, A. Kastrati, J. Mehilli, H. Schühlen, F. Dotzer, J. Hausleiter, M. Fleckenstein, F. J. Neumann, U. Sattelberger, C. Schmitt, M. Muller, J. Dirschinger, and A. Schömig. Intracoronary stenting and angiographic results: strut thickness effect on restenosis outcome (ISAR-STEREO-2) trial. *J. Am. Coll. Cardiol.*, 41:1283–1288, 2003.

[33] R. S. Schwartz and T. D. Henry. Pathophysiology of coronary artery restenosis. *Rev. Cardiovas. Med.*, 3, Suppl. 5:S4–S9, 2002.

[34] P. W. Serruys, P. de Jaegere, F. Kiemeneij, C. Macaya, W. Rutsch, G. Heyndrickx, H. Emanuelsson, J. Marco, V. Legrand, P. Materne, J. Belardi, U. Sijwart, A. Colombo, J. Goy, P. van den Heuvel, J. Delcan, and M. Morel. A comparison of balloon-expandable-

stent implantation with balloon angioplasty in patients with coronary artery disease.

Benestent Study Group. *N. Engl. J. Med.*, 331:489–495, 1994.

[35] H. C. Stary. *Atlas of Atherosclerosis: Progression and Regression*. The Parthenon Publishing Group, Boca Raton, London, New York, Washington, D.C., 2nd edition, 2003.

[36] L. A. Taber. Biomechanics of growth, remodelling, and morphogenesis. *Appl. Mech. Rev.*, 48:487–543, 1995.

[37] R. L. Taylor. *FEAP – A Finite Element Analysis Program, Version 7.5 User Manual*. University of California at Berkeley, Berkeley, California, 2005.

[38] D. L. Wang, B. S. Wung, Y. J. Shyy, C. F. Lin, Y. J. Chao, S. Usami, and S. Chien. Mechanical strain induces monocyte chemotactic protein-1 gene expression in endothelial cells. Effects of mechanical strain on monocyte adhesion to endothelial cells. *Circ. Res.*, 77:294–302, 1995.

[39] J. J. Wentzel, J. Kloet, I. Andhyiswara, J. A. Oomen, J. C. Schuurbiers, B. J. de Semet, M. J. Post, D. de Kleijn, G. Paterkamp, C. Borst, C. J. Slager, and R. Krams. Shear-stress and wall-stress regulation of vascular remodeling after balloon angioplasty: effect of matrix metalloproteinase inhibition. *Circulation*, 104:91–96, 2001.

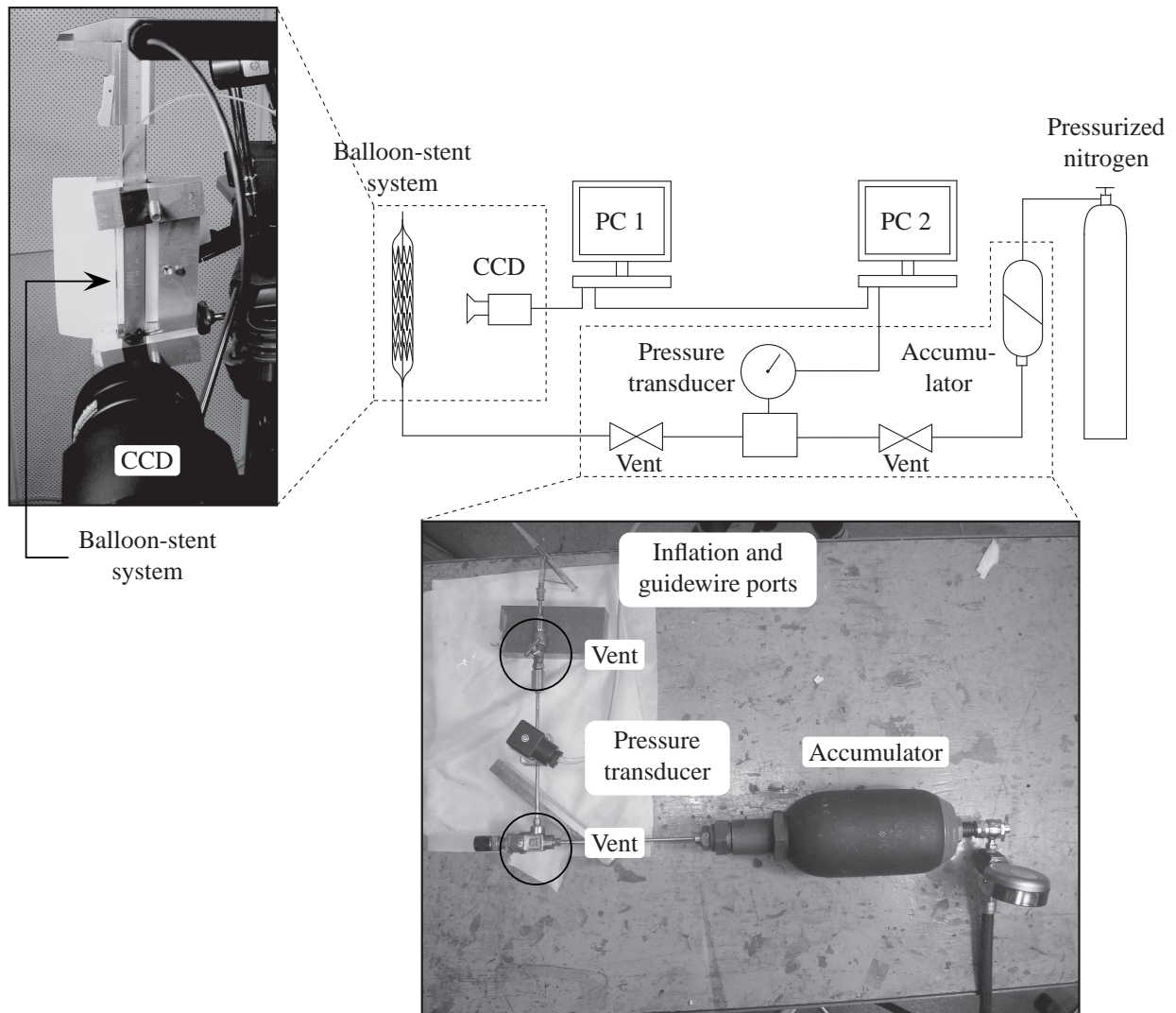


Figure 1: Schematic representation of the experimental setup used for the inflation of the balloon-expandable stents and for the recording of the load and deformation. The two photographs show various components of the setup.

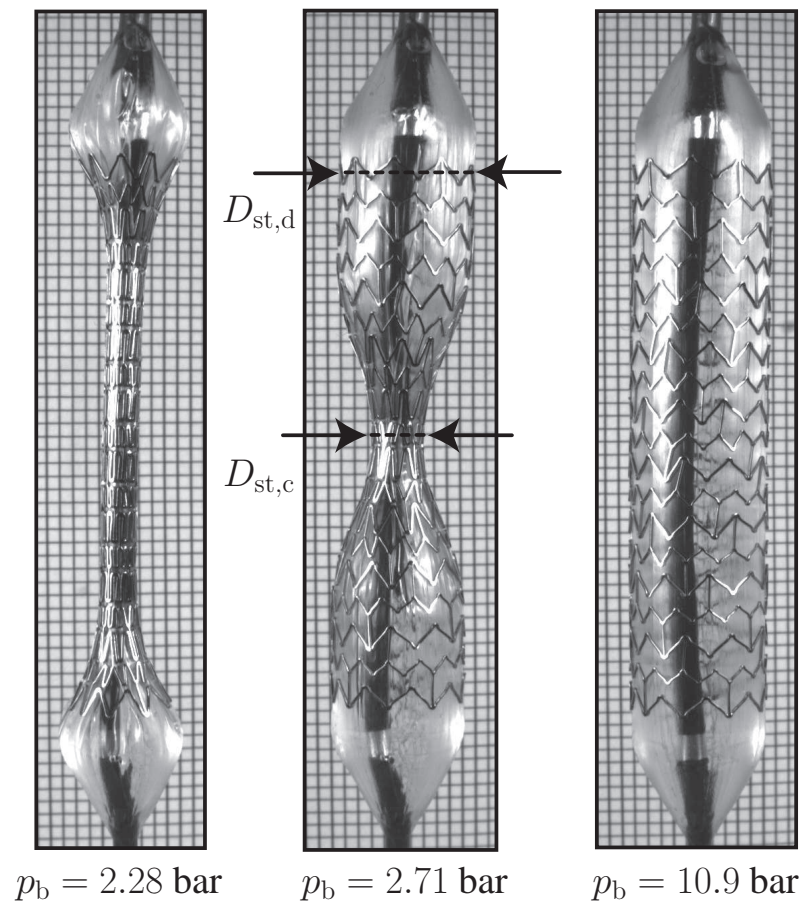


Figure 2: Three photographs taken during the inflation of an EXPRESS VASCULAR LD<sup>TM</sup> balloon-stent system. The deformed configurations of the balloon-catheter and the stent at three different inner balloon pressures  $p_b$  are displayed. From these images, and by means of image analysis software, the distal diameter  $D_{st,d}$  and the central diameter  $D_{st,c}$  of the stent were measured in addition to the total length. The dog-boning effect during the inflation of the balloon-expandable stent is clearly visible.

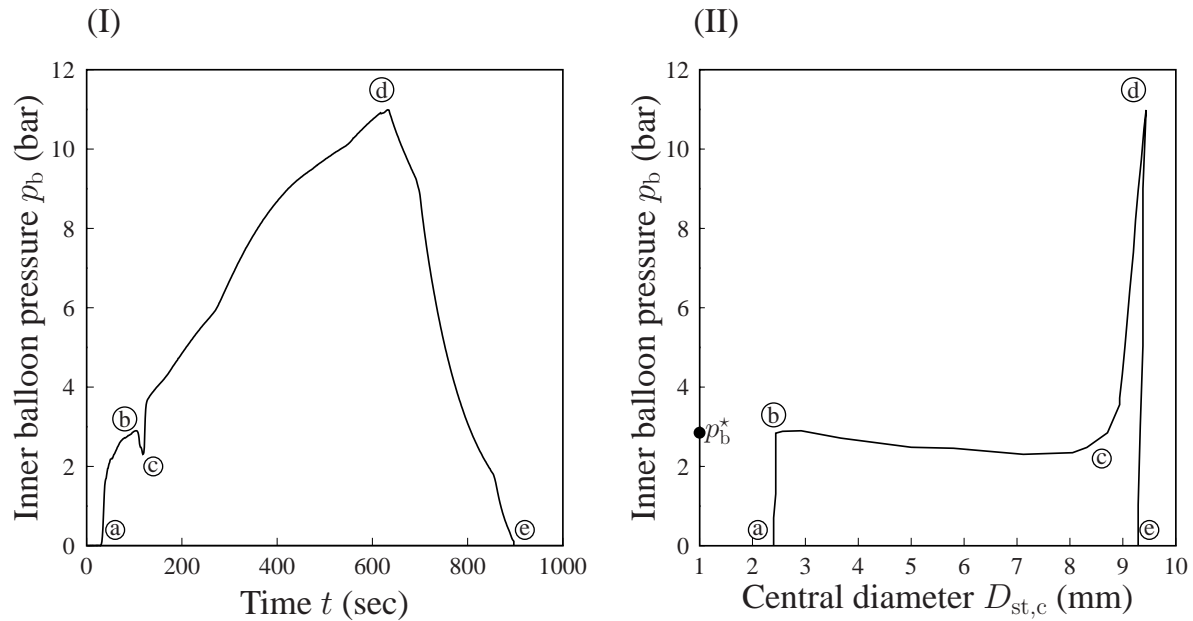


Figure 3: Change of the inner balloon pressure  $p_b$  over time  $t$  during inflation and deflation of an EXPRESS VASCULAR LD<sup>TM</sup> balloon-stent system (I). Change of the central diameter  $D_{st,c}$  of the stent over  $p_b$  (II). The deformation mechanism of balloon expandable stents is divided into four stages: (a)  $\rightarrow$  (b), balloon fitting and elastic stent deformation; (b)  $\rightarrow$  (c), burst opening accompanied with a large dilation rate; (c)  $\rightarrow$  (d), circumferential stiffening; (d)  $\rightarrow$  (e), load removal and (elastic) recoil.

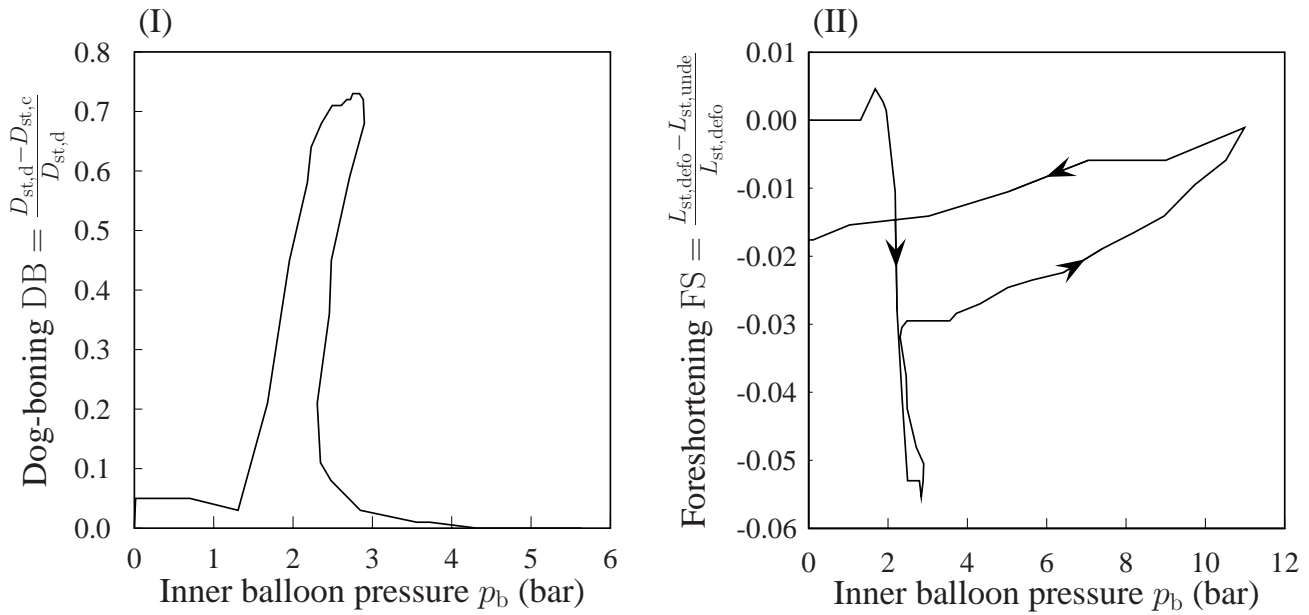


Figure 4: Phenomena that occur during the dilation of an EXPRESS VASCULAR LD<sup>TM</sup> stent: dog-boning DB (I) – the distal diameter  $D_{st,d}$  of the stent expands faster than the central diameter  $D_{st,c}$  until the burst opening of the central segments starts (at  $p_b^* = 2.90$  bar), and the stent obtains gradually a cylindrical shape; foreshortening FS (II) – during increase of the inner balloon pressure  $p_b$  the length  $L_{st,defo}$  of the stent initially shrinks. As the stent becomes cylindrical, it elongates, but does not reach its undeformed length  $L_{st,unde}$  in the fully deflated state.

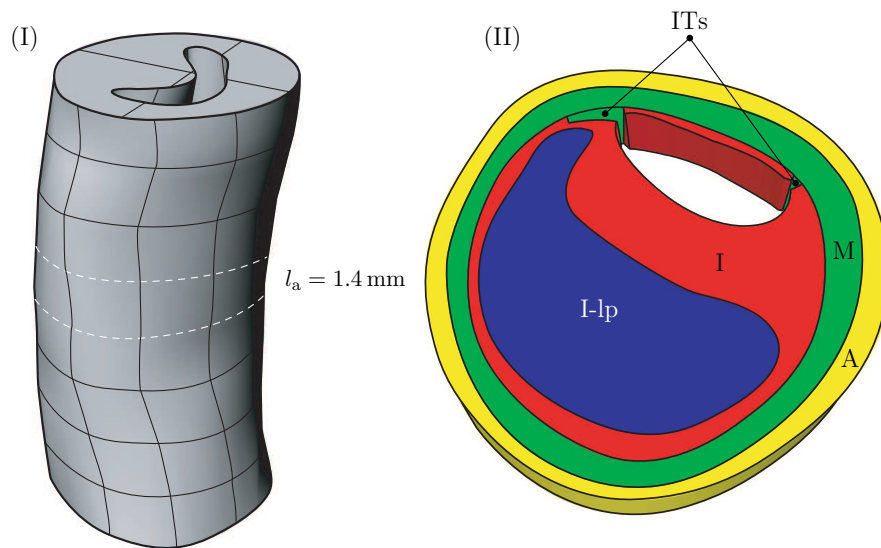


Figure 5: (I) 3D geometric model of a stenotic human iliac artery obtained from high-resolution MRI and reconstructed by means of NURBS. (II) Extracted arterial slice with length  $l_a = 1.4 \text{ mm}$ , composed by four arterial tissues: adventitia (A), media (M), intima (I) and lipid pool (I-lp). The introduced initial tears (ITs) are also indicated.

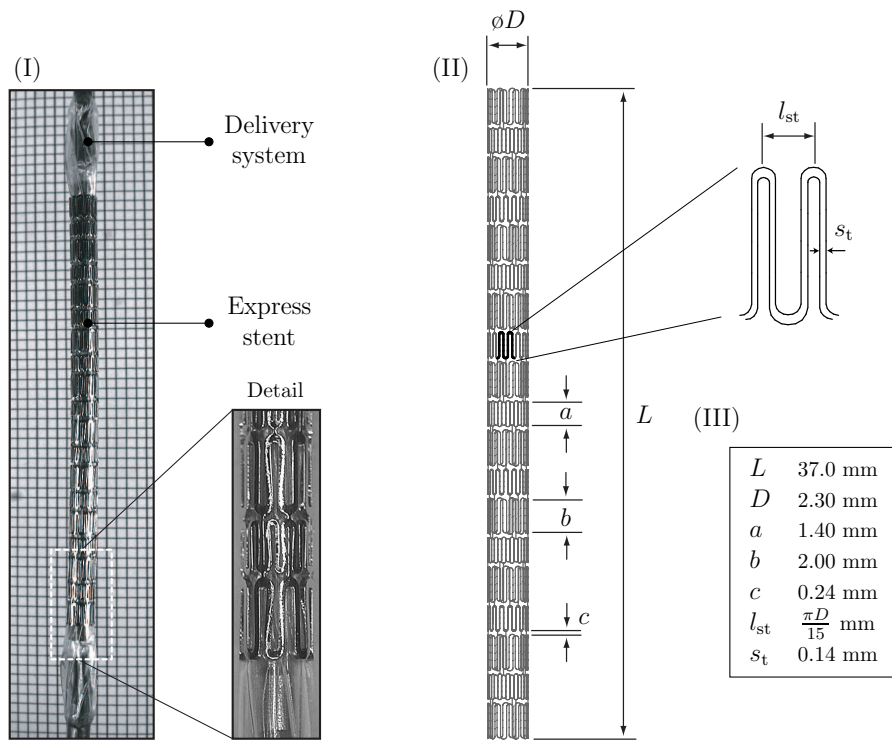


Figure 6: (I) Photograph of the undeformed configuration of the pre-mounted EXPRESS VASCULAR LD™ stent and detailed view of the stent's sinusoidal-structured cells. (II) 3D geometric model of the stent, obtained by a parametrization algorithm that makes use of the shown design parameters. (III) Dimensions of the obtained stent.

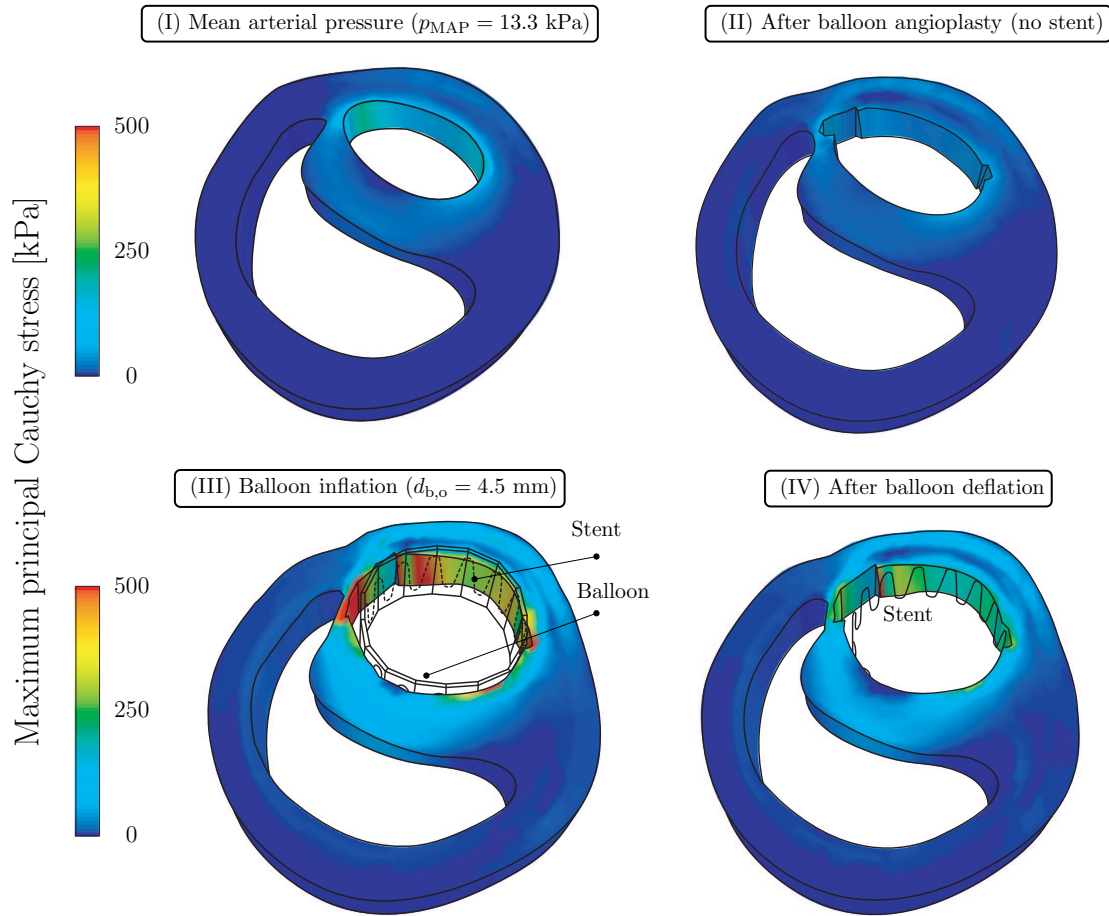


Figure 7: Deformed configuration and distribution of the maximum (principal) stresses in the arterial tissues (intima, media, adventitia) of an atherosclerotic human iliac artery at different load states: (I) mean arterial pressure ( $p_{\text{MAP}} = 13.3 \text{ kPa}$ ), no initial tears present; (II) balloon angioplasty without stenting; (III) balloon and stent inflation (up to  $d_{b,o} = 4.5 \text{ mm}$ ); (IV) after deflation of the balloon catheter (only the stent remains in contact with the arterial wall). The lipid pool is not shown.

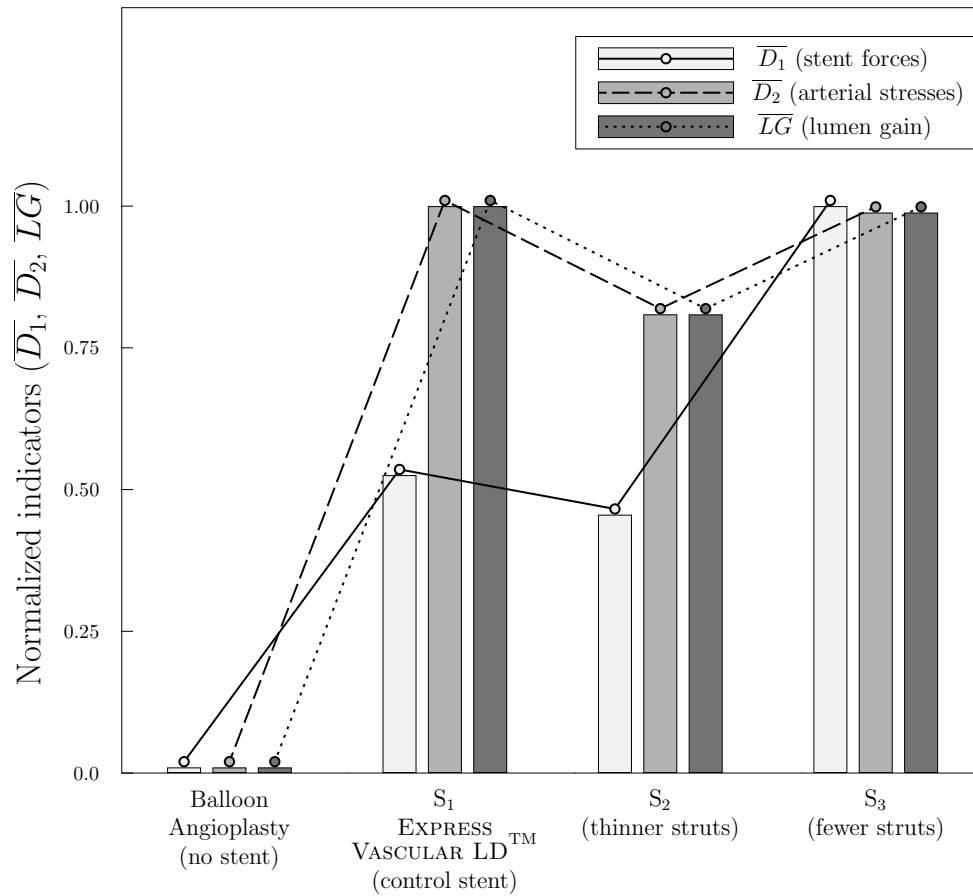


Figure 8: Normalized values of the indicators  $D_1$ ,  $D_2$ ,  $LG$  obtained from the performed simulations, i.e. ‘balloon angioplasty (no stent)’, ‘control stent  $S_1$ ’, ‘stent with thinner struts  $S_2$ ’ and ‘stent with fewer struts  $S_3$ ’ (parameters are according to Table 3). The indicators characterize the stent contact forces, the induced arterial stresses and the gain of lumen area, respectively.

Table 1: Experimental results obtained during and after the inflation and deflation of six commercially available balloon-expandable stent systems. The burst opening pressure  $p_b^*$  (in bar) for the central segments of each stent, the maximum values for the dog-boning  $DB_{\max}$  and the foreshortening  $FS_{\max}$ , according to (1) and (3), and the elastic recoil RE (in percent), according to (2), are given.

Product	$p_b^*$ (bar)	$DB_{\max}$ (-)	$FS_{\max}$ (-)	RE (%)
Express Vascular LD	2.90	0.73	-0.06	1.5
Express Vascular SD	4.35	0.67	-0.14	1.1
Palmaz Genesis	3.30	0.54	-0.04	3.8
Genesis Opti Pro	3.66	0.62	-0.10	0.1
Bridge Assurant	2.39	0.65	-0.05	4.5
Racer	3.32	0.52	+0.02	5.1

Table 2: Material and structural parameters of different tissue types, describing the anisotropic response of an atherosclerotic iliac lesion of type V. Data taken from Holzapfel et al.<sup>19</sup>

Tissue	$\mu$ (kPa)	$k_1$ (kPa)	$k_2$ (-)	$\alpha$ (°)
Adventitia (A)	1.75	65.6	61.8	$\pm 49.0$
Media (M)	15.0	4.0	2.3	$\pm 7.0$
Intima (I)	78.9	23.7	26.3	0.0
Lipid Pool (I-lp)	0.1	0.0	-	-

Table 3: Values of the geometric parameters of the three different stent designs used in the simulations of balloon angioplasty with stenting. The value of the diameter  $D$  is given in Fig. 6.

Stent configurations	$s_t$ (mm)	$l_{st}$ (mm)
$S_1$ (control stent)	0.14	$\pi D/15$
$S_2$ (thinner struts)	0.10	$\pi D/15$
$S_3$ (fewer struts)	0.14	$\pi D/7$